Technical Report 589

K-P. Dunn

Accuracy of Parameter Estimates for Closely Spaced Optical Targets Using Multiple Detectors

23 October 1981

Prepared for the Department of the Army
under Electronic Systems Division Contract F19628-80-C-0002 by

Lincoln Laboratory
MASSACHUSETTS INSTITUTE OF TECHNOLOGY
LEXINGTON, MASSACHUSETTS

The work reported in this document was performed at Lincoln Laboratory, a center for research operated by Massachusetts Institute of Technology. This program is sponsored by the Ballistic Missile Defense Program Office, Department of the Army; it is supported by the Ballistic Missile Defense Advanced Technology Center under Air Force Contract F19628-80-C-0002.

Raymond L. Loiselle

Raymond L. Loiselle, Lt. Col., USAF
Chief, ESD Lincoln Laboratory Project Office

MASSACHUSETTS INSTITUTE OF TECHNOLOGY
LINCOLN LABORATORY

ACCURACY OF PARAMETER ESTIMATES FOR CLOSELY SPACED OPTICAL TARGETS USING MULTIPLE DETECTORS

K-P. DUNN
Group 32

TECHNICAL REPORT 589

23 OCTOBER 1981

LEXINGTON MASSACHUSETTS

ABSTRACT

In order to obtain the cross-scan position of an optical target, more than one scanning detectors are used. As expected, the cross-scan position estimation performance degrades when two nearby optical targets interfere with each other. Theoretical bounds on the two-dimensional parameter estimation performance for two closely spaced optical targets are found. Two particular classes of scanning detector arrays, namely, the crcw's foot and the brickwall (or mosaic) patterns, are considered.

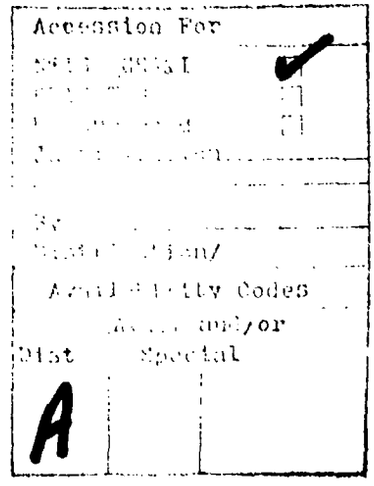

CONTENTS

I. INTRODUCTION

Recently, considerable attention has been focused upon the accuracy of parameter estimates of an optical system for closely spaced objects (CSOs) [1] - [7]. The intensity and location information of an optical image on the sensor focal plane is collected by a scanning detector as shown in Fig. 1. The detector output, a time function, is a convolution of the optical image (which contains intensity and location information) and the detector response. There are various types of noise sources at the output of the detector, therefore estimating the image position and intensity from the noisy output can not be errorless. Theoretical lower bounds on the accuracy of parameter estimates have been derived in [1] - [4].

The Cramer-Rao lower bound technique is used in [2] - [4] to calculate the best achievable performance of any unbaised estimator of the unknown parameters. The results presented in [1] are obtained using a different error analysis technique. Other than some numerical problems pointed out in [4], which occurred at small target separations, the approach presented in [1] should have results identical to those obtained by the Cramer-Rao lower bound approach. There are algorithms developed to perform the parameter estimation for closely spaced objects from noisy measurements, for example [5] - [7]. Monte Carlo simulation results are presented in [5] and [7]. In [5], the well known

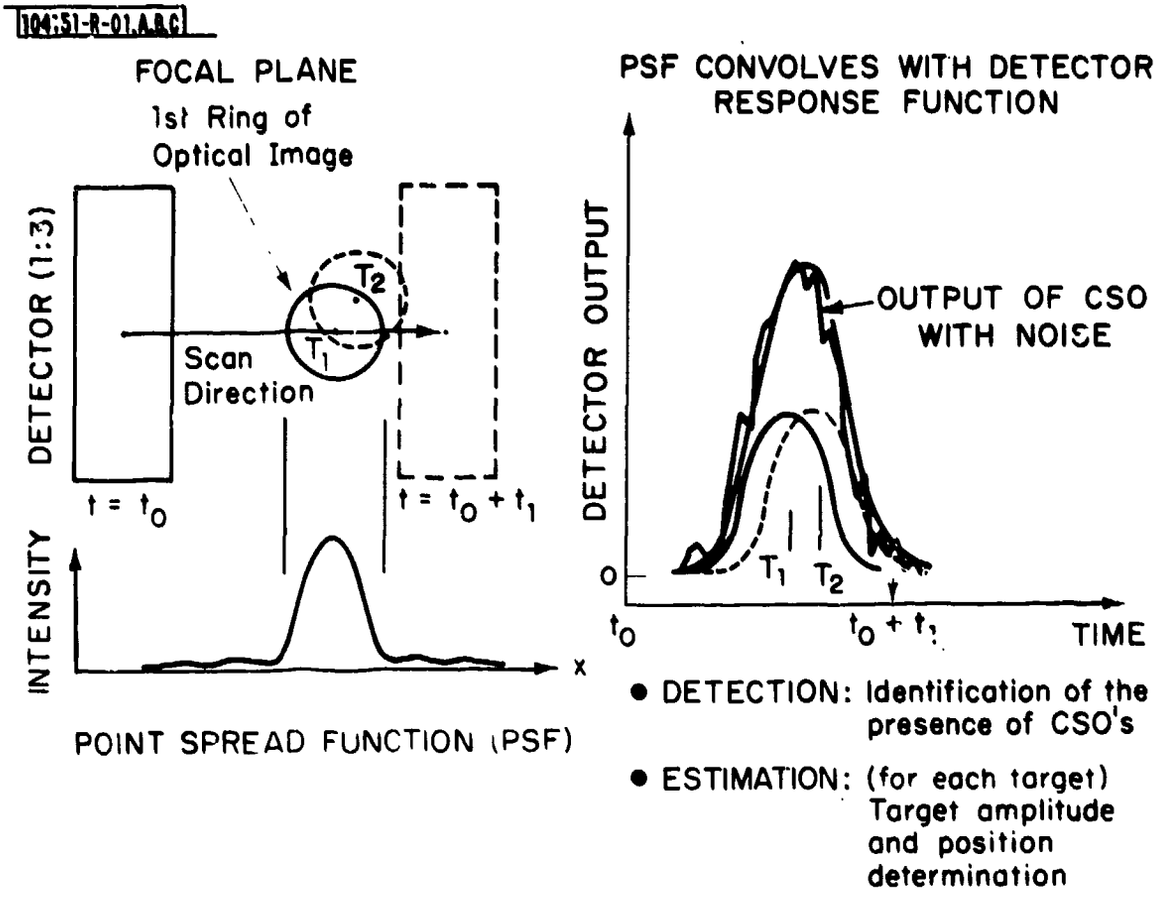

Fig. 1. Closely spaced object (CSO) resolution problem for optical system with scanning detector.

maximum-likelihood estimator is implemented for parameter estimation and the Akaike information criterion [8] is employed to estimate the number of targets in the CSO cluster.

All analytical and simulation results presented in the past pertain only to the in-scan direction and assume a vertical rectangular detector as shown in Fig. 1. Many detector array arrangements have been considered by sensor designers to obtain position information of a single optical target in the cross-scan direction. Some typical detector patterns considered are shown in Fig. 2. The time between detector crossings for the chevron and crows's foot patterns can be used to determine the cross-scan position of the target. With two targets, this problem becomes more difficult. Figure 3 shows three individual detector outputs of a crow's foot pattern for different orientations of target locations. It is obvious that with one linear detector (detector M) output alone, one can not obtain cross-scan position information. From the results we have presented in [2] - [5], one can obtain in-scan position information of two CSOs no matter how close they are if the detector output is noise free. It is, however, not true for a noisy output; the estimation errors increase drastically as the CSO separation decreases. For the chevron pattern (detectors L and R), the cross-scan position information can be obtained without error from noise free outputs for all target locations. For noisy outputs, there are target locations, for example, case II of

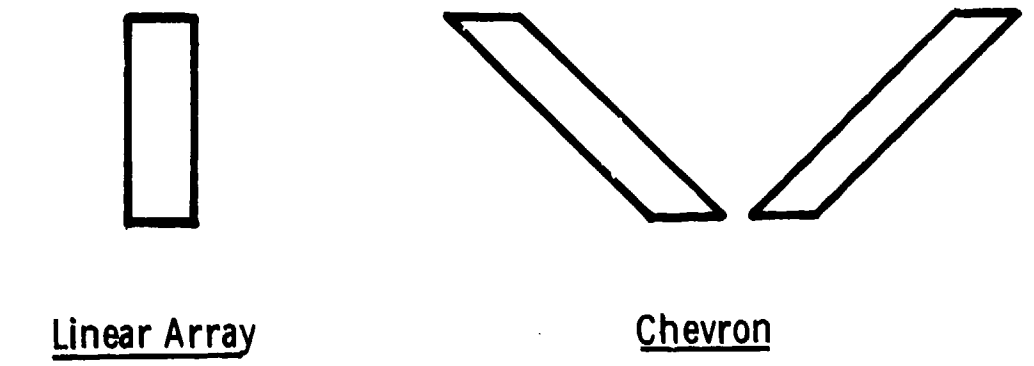

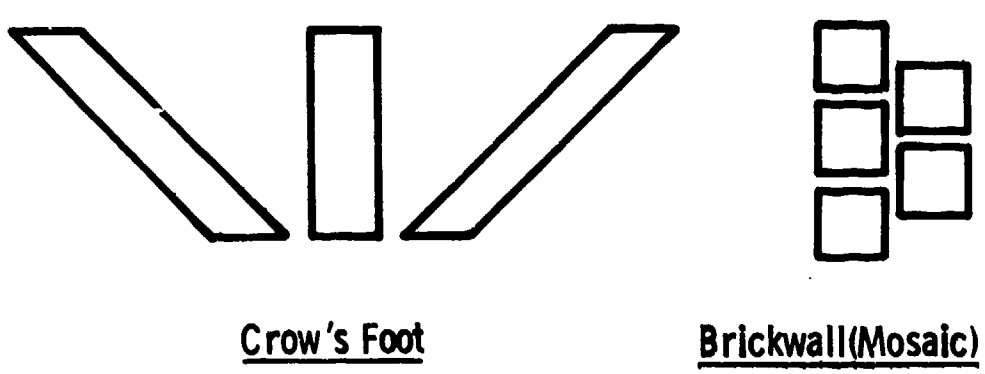

Fig. 2. Typical detector patterns have been considered.

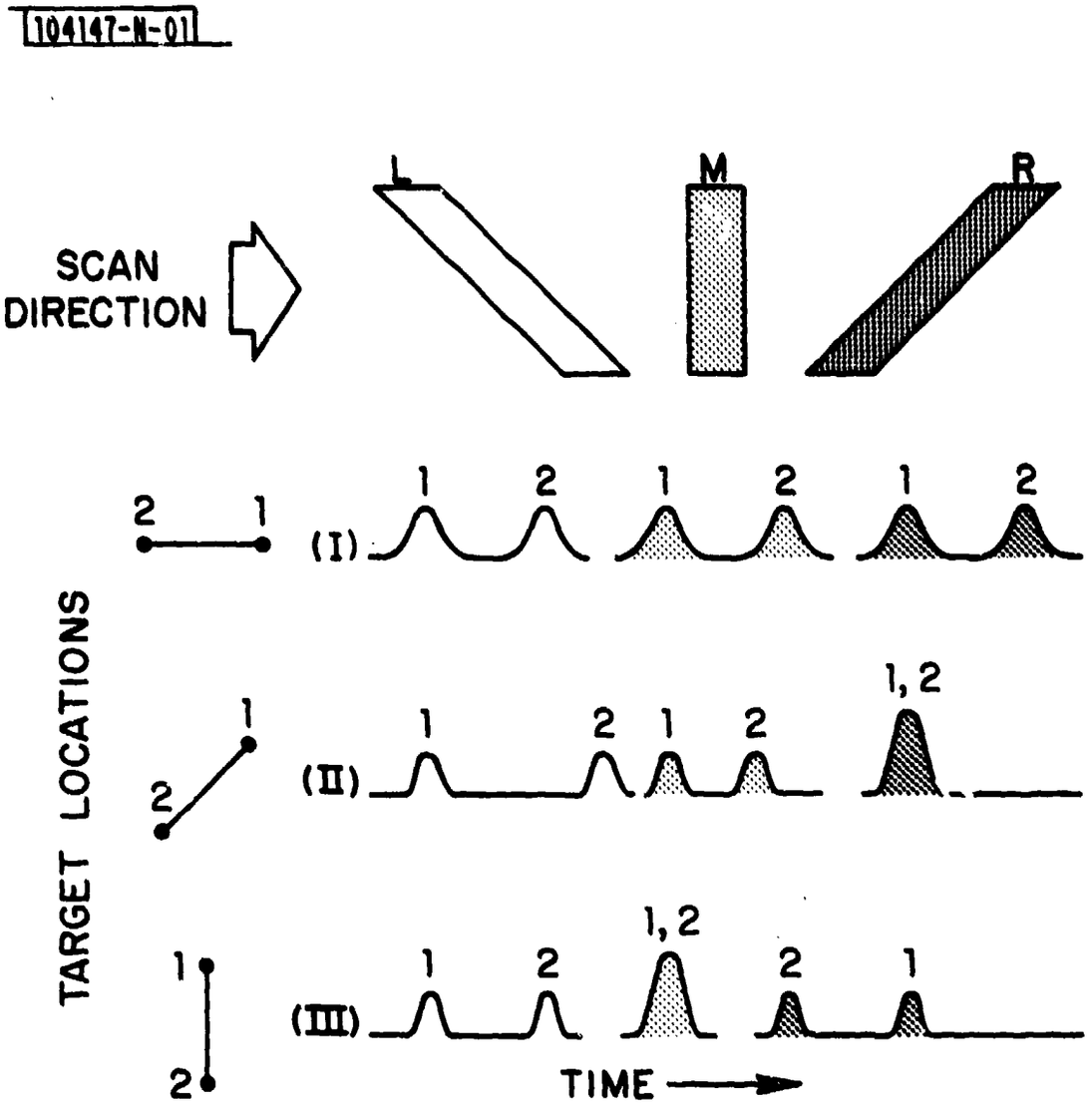

Fig. 3. Individual detector outputs of a crow's foot pattern for different orientations of target locations.

Fig. 3, where the target position estimation errors may be very large no matter how large the actual target separation is. This is because there is a CSO situation for the detector R. A more complicated detector array arrangement may solve this problem, for example the crow's foot pattern shown in Fig. 3. The achievable estimation performance of the cross-scan position of two CSOs for these particular detector patterns has not been studied analytically previously. It is the purpose of this report to derive the Cramer-Rao lower bounds on the variance of parameter estimates as a function of both scan and cross-scan separations for CSOs measured by detector patterns shown in Fig. 2. The performance bounds presented in this report are derived with the assumption that all detector outputs are utilized optimally for unbiased parameter estimation; no particular signal processing procedure has been adopted in the analysis.

The general formulation of this problem and its associated Cramer-Rao bounds are presented in the next section. In Section III, results for linear, chevron, and crow's foot arrays using a particular optical point spread function are presented. For other point spread functions and detector widths, one can utilize the formulas provided in Appendix A to calculate the associated estimation performance bounds. In Section IV, the brickwall (or mosaic) detector patterns are considered. Some typical results for the same point spread function considered in Section III are pre-

sented. Formulas that can be used to calculate the estimation performance bounds are provided in Appendix B. A summary and conclusions are given in Section V.

II. ANALYSIS

Let us assume there is an array of M detectors in the focal plane of a scanning optical sensor; some typical patterns of these detectors are shown in Fig. 2. Let (x_k, y_k) be the center and θ_k be the orientation of the kth detector with the center of the focal plane scanning along the x-axis as shown in Fig. 4. Let $p_k(t,x,y)$ be the output of the kth detector to a unit strength point source located at (x,y) at t=0.† A point source is called a unit strength point source, if for $(x,y)=(x_k,y_k)$ and $\theta_k=90°$, the output signal $p_k(t,x,y)$ satisfies:

$$\int_{-\infty}^{\infty} p_k^2(t,x,y)dt = 1. \qquad (1)$$

It is important to note that, $p_k(t,x,y)$ is a convolution of the point source blurred image (e.g., point spread function, PSF, for a monochromatic source) on the focal plane and the response of the kth detector. In general, it is a complicated function of the detector location (x_k, y_k) shape, orientation (θ_k), and the instantaneous target location (x-t,y) on the focal plane at time t. A single point source located at (x,y) with amplitude a will

†In the remainder of this note, a point source (or, target) location is always referred to its location on the focal plane at t=0.

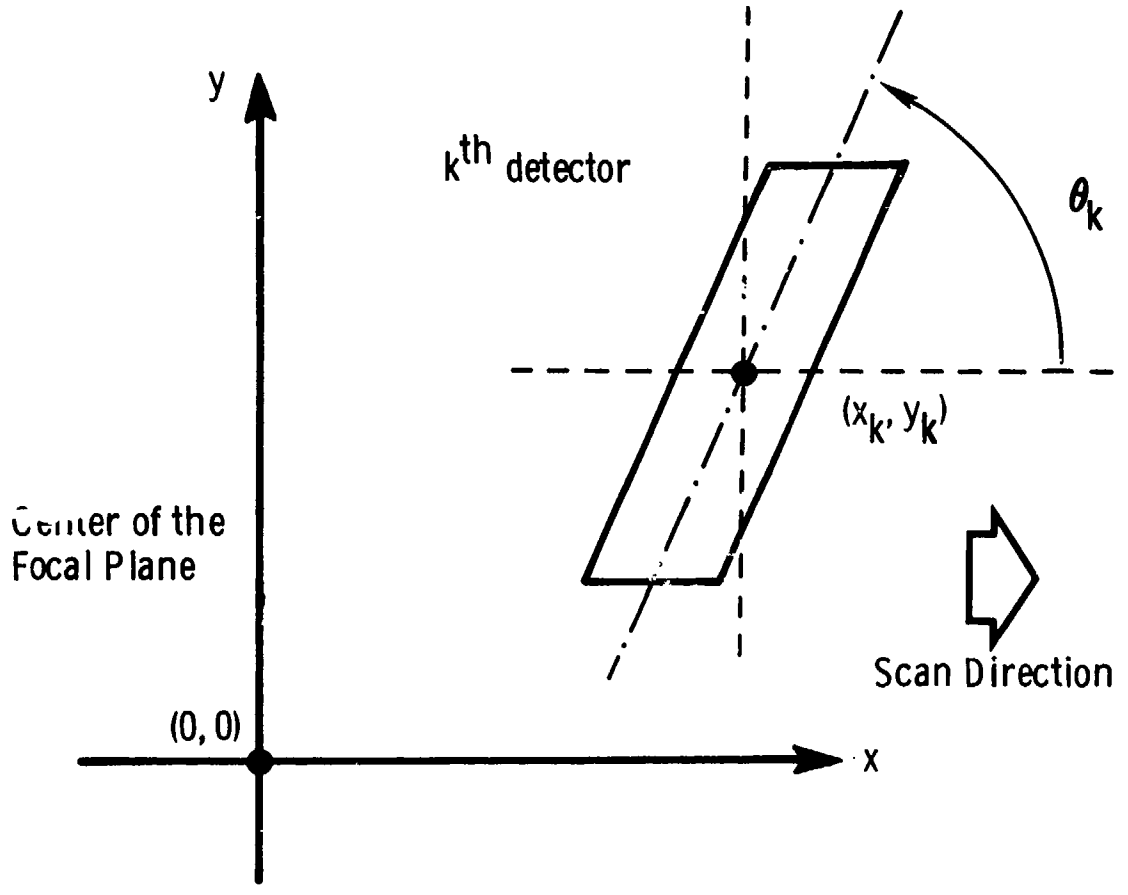

Fig. 4. Individual detector location with respect to the center of focal plane and its orientation with respect to the scanning direction.

have a noiseless output

$$s_k(t) = ap_k(t,x,y) \tag{2}$$

at the kth detector at time t.

The problem treated here concerns the measurements of a pair of point sources from the output of an M detector array. Let $(a_1, (\bar{x}_1, \bar{y}_1))$ and $(a_2, (\bar{x}_2, \bar{y}_2))$ be the amplitude and location of the point sources. The noiseless output of the kth detector can be written as the following:

$$s_k(t) = a_1 p_k(t,\bar{x}_1,\bar{y}_1) + a_2 p_k(t,\bar{x}_2,\bar{y}_2). \tag{3}$$

We wish to determine $(a_i, (\bar{x}_i,\bar{y}_i))$, i=1,2 from noisy measurements, taken at the output of each detector, i.e.,

$$y_k(t) = s_k(t) + n_k(t), \quad k=1,2,\ldots,M, \tag{4}$$

where $n_k(t)$ is a white Gaussian noise with two-sided power spectrum density $N_o/2$. Furthermore, these noises are mutually independent, that is

$$E[n_i(t)n_j(\tau)] = 0, \quad \text{for all } t \text{ and } \tau, \text{ when } i \neq j. \tag{5}$$

The Cramer-Rao lower bound on the variance of any unbaised estimator of the unknown parameters: amplitude of object 1, a_1, amplitude ratio, $R = a_2/a_1$, location of object 1, $(\bar{x}_1,\bar{y}_1)$, separation, r, and orientation of objects, θ (the angle between the detector scan direction and the vector $(\bar{x}_2,\bar{y}_2) - (\bar{x}_1,\bar{y}_1)$, as shown

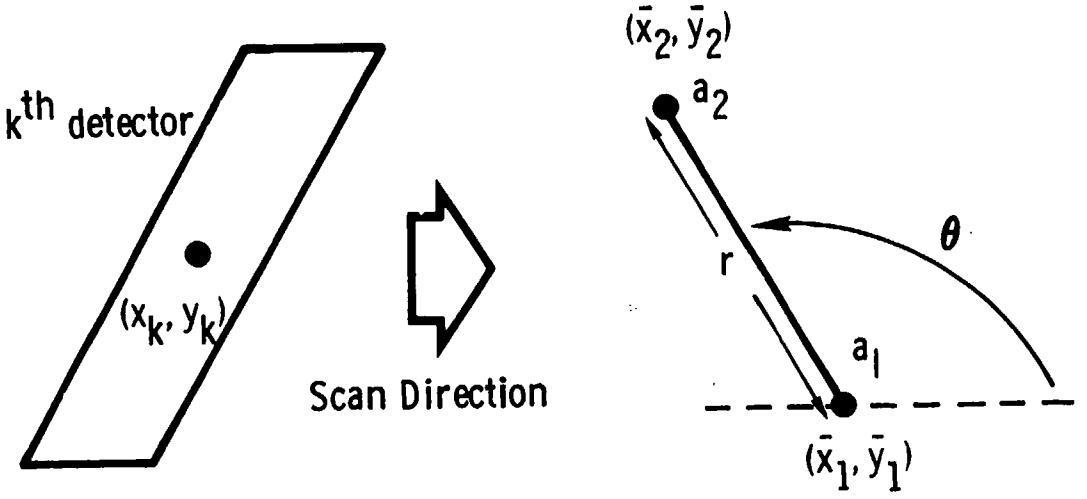

R = Amplitude Ratio = a_2 / a_1

Fig. 5. Unknown parameters of a pair of CSOs.

in Fig. 5, can be obtained by inverting the Fisher information matrix, F, whose (i,j)th element is [9]

$$F_{ij} = E\left\{\frac{\partial \ln \Lambda}{\partial \alpha_i} \quad \frac{\partial \ln \Lambda}{\partial \alpha_j}\right\} \tag{6}$$

where α_i denotes the ith unknown parameter, namely, $\alpha_1=a_1$, $\alpha_2=R$, $\alpha_3=\bar{x}_1$, $\alpha_4=\bar{y}_1$, $\alpha_5=r$ and $\alpha_6=\theta$, and where ln Λ is the log likelihood ratio [9, p. 274]

$$\ln \Lambda = \frac{1}{N_o}\left\{2\int_{-\infty}^{\infty} y^T(t)s(t)dt - \int_{-\infty}^{\infty} s^T(t)s(t)dt\right\}, \tag{7}$$

and

$$s(t)=\begin{bmatrix} s_1(t) \\ s_2(t) \\ \cdot \\ \cdot \\ s_M(t) \end{bmatrix} \quad , \quad y(t)=\begin{bmatrix} y_1(t) \\ y_2(t) \\ \cdot \\ \cdot \\ y_M(t) \end{bmatrix} \quad . \tag{8}$$

Substituting (7) and (8) into (6), and using the statistical model of the problem described in (4) and (5), we have

$$F_{ij} = \frac{2}{N_0}\left\{\sum_{k=1}^{M}\int_{-\infty}^{\infty}\left(\frac{\partial s_k(t)}{\partial \alpha_i}\right)\left(\frac{\partial s_k(t)}{\partial \alpha_j}\right) dt\right\}. \tag{9}$$

Having an explicit expression for the output function $p_k(t,\bar{x}_i,\bar{y}_i)$, i=1,2 and k=1,2,...,M, one can compute F_{ij} according to (9). In the following sections we will consider two simple cases where the partial derivatives, $\partial s_k(t)/\partial \alpha_i$, i=1,...,6, can be obtained explicitly.

III. LINEAR, CHEVRON, AND CROW'S FOOT DETECTOR ARRAYS

In this section, a special class of detector patterns is considered. The detector array consists of M parallogram detectors with the shorter width along the scan direction as shown in Fig. 2. The detector pattern is called a linear array if all $\theta_k=90°$, a chevron array if θ_k takes only two values, one greater than and one less than 90°, and crow's foot if θ_k takes three values (i.e., a combination of linear and chevron arrays). For simplicity in the analysis, let us make the following assumptions:

1) the center of each detector is located along the scan axis, i.e., $y_k=0$ for all k.

2) the output of each detector to a unit strength point source located at (x,y) has the same functional form:†

$$p_k(t,x,y) = p(t-(x-x_k) + y \cot\theta_k), \tag{10}$$

where $p(\cdot)$ is a symmetric, non-negative-valued function. Furthermore, let $\rho(t)$ be the autocorrelation function of $p(t)$,i.e.,

$$\rho(t) = \int_{-\infty}^{\infty} p(\tau)p(\tau-t)d\tau. \tag{11}$$

It is easy to see that $\rho(0)=1$ from the definition of $p_k(t,x,y)$ in (1).

Rewriting (3) in terms of the parameters considered in Section

†This implicitly assumes that the detector has infinite length or no edge effects on the detector output.

II with the above assumptions, we obtain

$$s_k(t) = a_1 p\left(t-(\bar{x}_1-x_k) + \bar{y}_1\cot\theta_k\right) + a_1 R p\left(t-(\bar{x}_1+r\cos\theta-x_k) + (\bar{y}_1+r\sin\theta)\cot\theta_k\right). \quad (12)$$

Substituting (12) into (9), we have F_{ij} in terms of the following functions:

$$\rho(\tau) = \int_{-\infty}^{\infty} p(t)\ p(t-\tau)dt \quad (13)$$

$$\dot{\rho}(\tau) = -\int_{-\infty}^{\infty} p(t)\dot{p}(t-\tau)dt \quad (14)$$

and

$$\ddot{\rho}(\tau) = -\int_{-\infty}^{\infty} \dot{p}(t)\dot{p}(t-\tau)dt \quad (15)$$

The expression of each element of F is given in Appendix A.

The lower bounds on the variances of the estimates for a_1, R, $\bar{x}_1$, $\bar{y}_1$, r, and θ are:

$$\text{CRB}\ (a_1) = (F^{-1})_{11} \quad (16a)$$

$$\text{CRB}\ (R) = (F^{-1})_{22} \quad (16b)$$

$$\text{CRB}\ (\bar{x}_1) = (F^{-1})_{33} \quad (16c)$$

$$\text{CRB}\ (\bar{y}_1) = (F^{-1})_{44} \quad (16d)$$

$$\text{CRB}\ (r) = (F^{-1})_{55} \quad (16e)$$

$$\text{CRB}\ (\theta) = (F^{-1})_{66} \quad (16f)$$

The results in this report are presented in the following normalized forms:

$$E_a \triangleq \sqrt{CRB(a_1)}/a_1 \tag{17a}$$

$$E_R \triangleq \sqrt{CRB(R)}/R \tag{17b}$$

$$E_x \triangleq \sqrt{CRB(\bar{x}_1)}/d_x \tag{17c}$$

$$E_y \triangleq \sqrt{CRB(\bar{y}_1)}/d_x \tag{17d}$$

$$E_r \triangleq \sqrt{CRB(r)}/r \tag{17e}$$

$$E_\theta \triangleq \sqrt{CRB(\theta)}, \tag{17f}$$

where d_x is the detector width in the scan direction. All results will be presented at SNR_1=10 for each detector, where

$$SNR_1 \triangleq a_1/\sigma_a \tag{18a}$$

and

$$\sigma_a \triangleq \left[\int_{-\infty}^{\infty} p^2(t)dt\right]^{1/2} = 1. \tag{18b}$$

It is easy to convert these results to any signal-to-noise ratio, SNR, by the following relationship:

$$E_\omega \text{ at SNR} = (E_\omega \text{ at } SNR_1=10) \times (10/SNR) \tag{19}$$

where ω = a, R, $\bar{x}_1$, $\bar{y}_1$, r, and θ.

For the numerical results presented here, let us consider that

the function $p(\cdot)$ is generated by convolving an infinite length rectangular detector of width, d_x, along the scan direction with a point spread function of the form [10]

$$s_f(x,y) = \frac{E}{2\pi\sigma^2} \exp\left\{ - \frac{(x-x_o)^2 + (y-y_o)^2}{2\sigma^2} \right\}, \qquad (20)$$

where E is the image irradiance at the center of the diffraction pattern and

$$\sigma = .3040\ d_x. \qquad (21)$$

The value of σ is selected such that 90% of the total energy is collected by a detector centered at (x_o, y_o).

Figures 6a and 6b present the Cramer-Rao bounds on the estimation errors for a linear array detector (detector M in Fig. 2) for the amplitude, a_1, and the in-scan location, $\bar{x}_1$, respectively. The upper half of each figure is the Cramer-Rao bound computed for the 1-D problem, in our previous reports [2] - [4], where targets are located along the scan axis. The lower half of each figure shows the equal performance contours plotted on the sensor focal plane for the 2-D problem with one target at the origin and the other at position (x,y). Because the detector pattern is scanning along the x-axis, the equal performance contours plotted in the lower half of each figure are symmetric about the cross-scan axis (y-axis). This symmetric property is in common to all figures shown in this report. Notice that the equal performance

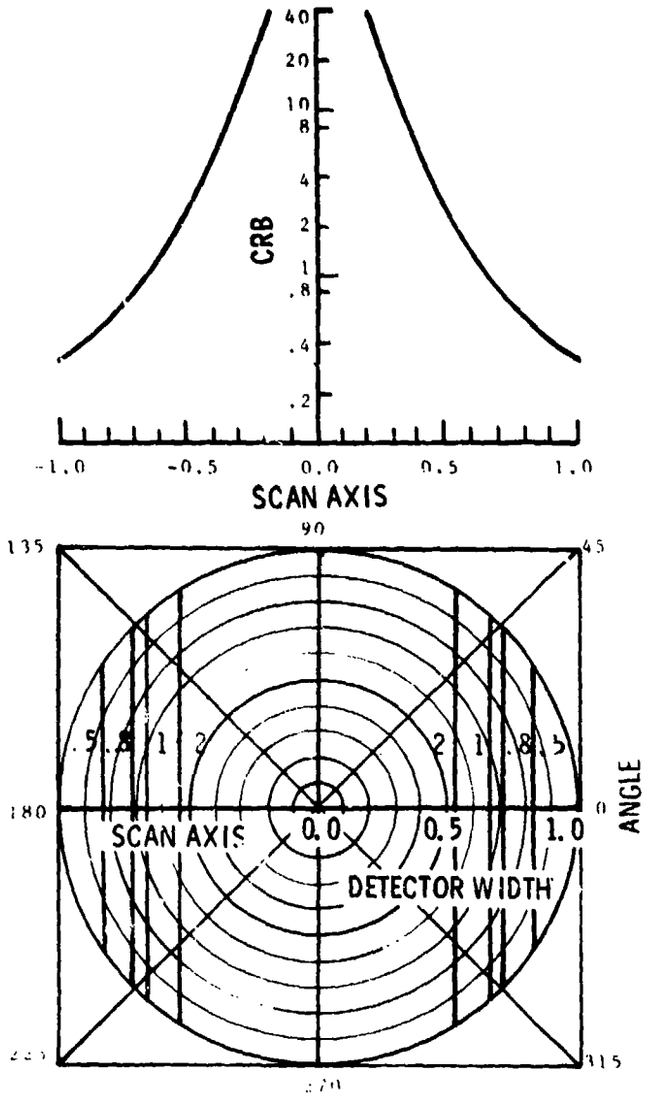

CRAMER-RAO BOUNDS ON a_1 (FRACTION OF a_1)

Fig. 6a. The Cramer-Rao bound on the amplitude estimation errors for a linear array detector.

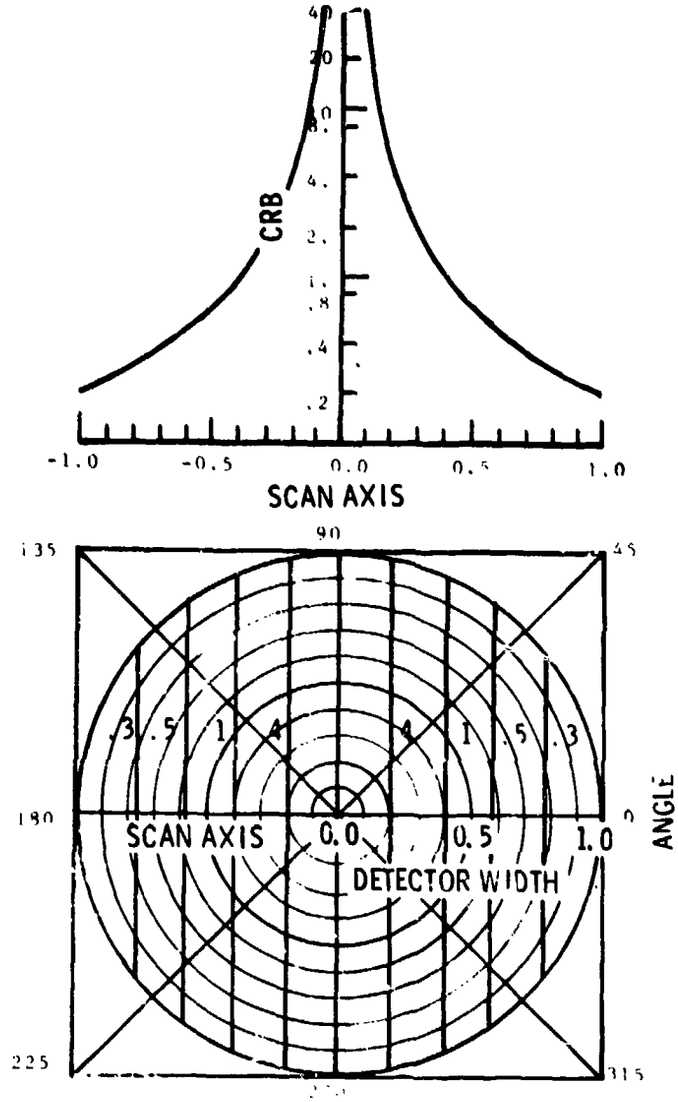

Fig. 6b. The Cramer-Rao bound on the in-scan location estimation errors for a linear array detector.

contours in these figures (6a and 6b) are independent of the y component of the second target location. It indicates that there is no way one can obtain cross-scan position information from the output of a single detector alone. In Fig. 6b, we see that the CRB's go to infinity as the true separation goes to zero. This is correct for an unbiased estimator; however (biased) algorithms exist which produce finite errors at zero separation. Not considered here but of great importance for CSO's is the CSO detection problem (see Ref. 5). At small separations, it is equally difficult to recognize that there are two unresolved targets as it is to estimate their parameters assuming that there are two targets. The singularity in estimation error at zero separation will be seen to influence the performance bounds for more complicated detector patterns later in this section.

Figures 7a and 7b present the Cramer-Rao bounds on the estimation errors for a chevron array (detectors L and R in Fig. 3) for the amplitude, a_1, and the orientation of objects, θ, respectively. The upper half of each figure is a plot of the surface formed by the Cramer-Rao bound, which is a function of the second target position (x,y). The surface is cut-off at a fixed value. The edge of the plateau forms the innermost equal value contour on the lower half of the figure. The value of the Cramer-Rao bound approaches infinity as the (x,y) position approaches (0,0). Note that the maplitude estimation error does not approach infinity except at the origin

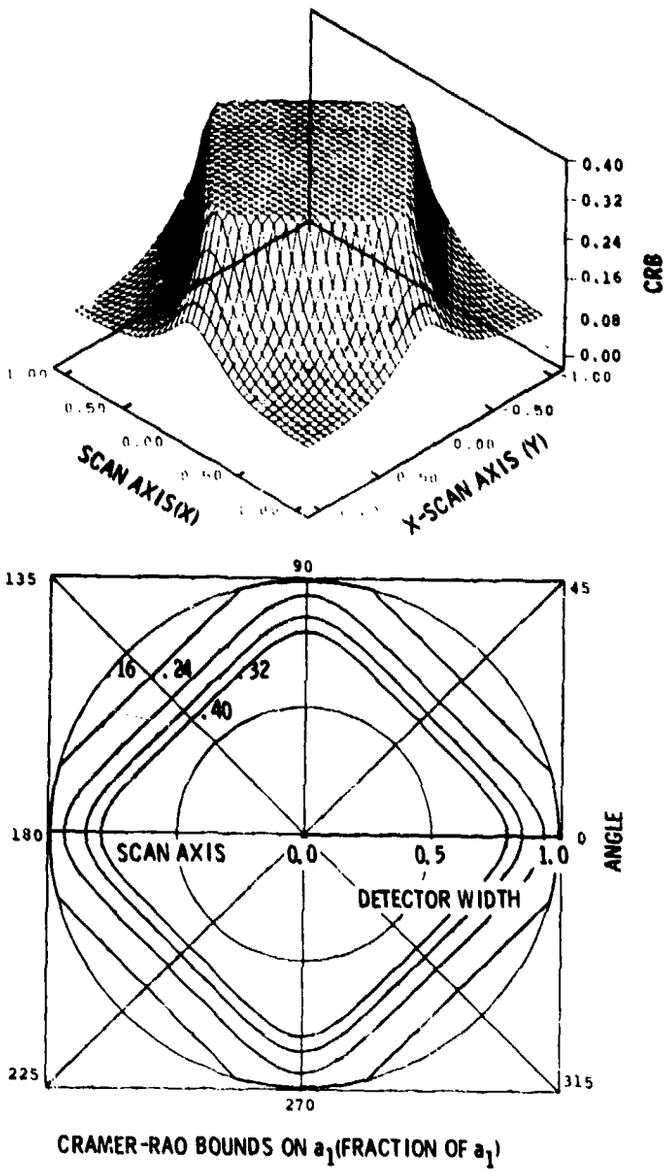

Fig. 7a. The Cramer-Rao bound on the amplitude estimation errors for chevron detector pattern.

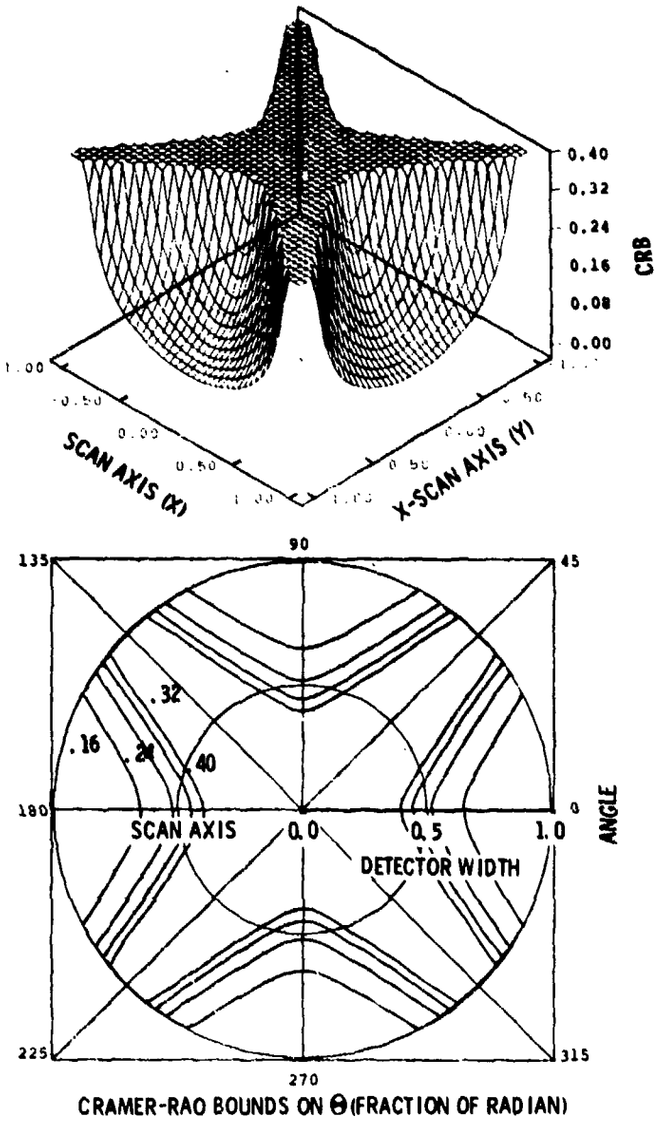

Fig. 7b. The Cramer-Rao bound on the CSO orientation estimation errors for a chevron detector pattern.

(where the two targets are colocated), while the estimation error for the orientation of the objects approaches infinity at target orientations aligned with either one of the detectors. Since the target separation is zero for one detector, the CRB on estimation errors for that detector is infinite. For orientation estimation, information from both detectors is required resulting in infinite error for an unbiased estimator of θ. As with a single detector, this is a reflection of the CSO recognition problem. For amplitude estimation, it is sufficient to use information obtained from the detector which does not have CSO interference.

Figure 8a to Figure 8f present the Cramer-Rao bounds on the normalized estimation errors defined in Eqs. (17a) - (17f), respectively, for the crow's foot detector (detectors L, M, and R in Fig 3). A similar format to the results shown in Fig. 7a and 7b is used. One thing in common to all these figures is that the errors increase monotonically toward the center (0,0) but none of these parameters has errors approaching infinity except at the origin. As seen in Fig. 3, for any target orientation, there will always be at least two detectors which measure a nonzero separation. Since all parameters can be estimated using information from two detectors, there are no singularites as was the case for the chevron pattern.

The shape of the contours shown in Figs. 8a - 8f can be explained by the following heuristic argument: The estimation

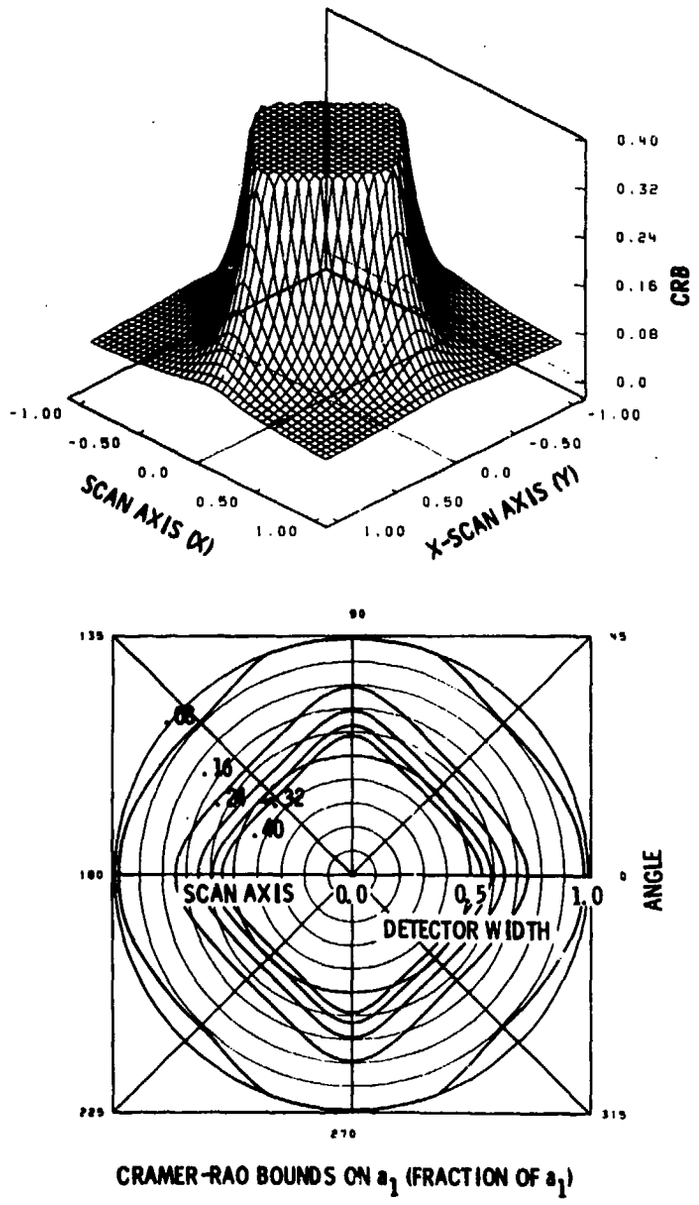

Fig. 8a. The Cramer-Rao bound on the amplitude estimation errors for a crow's foot detector pattern.

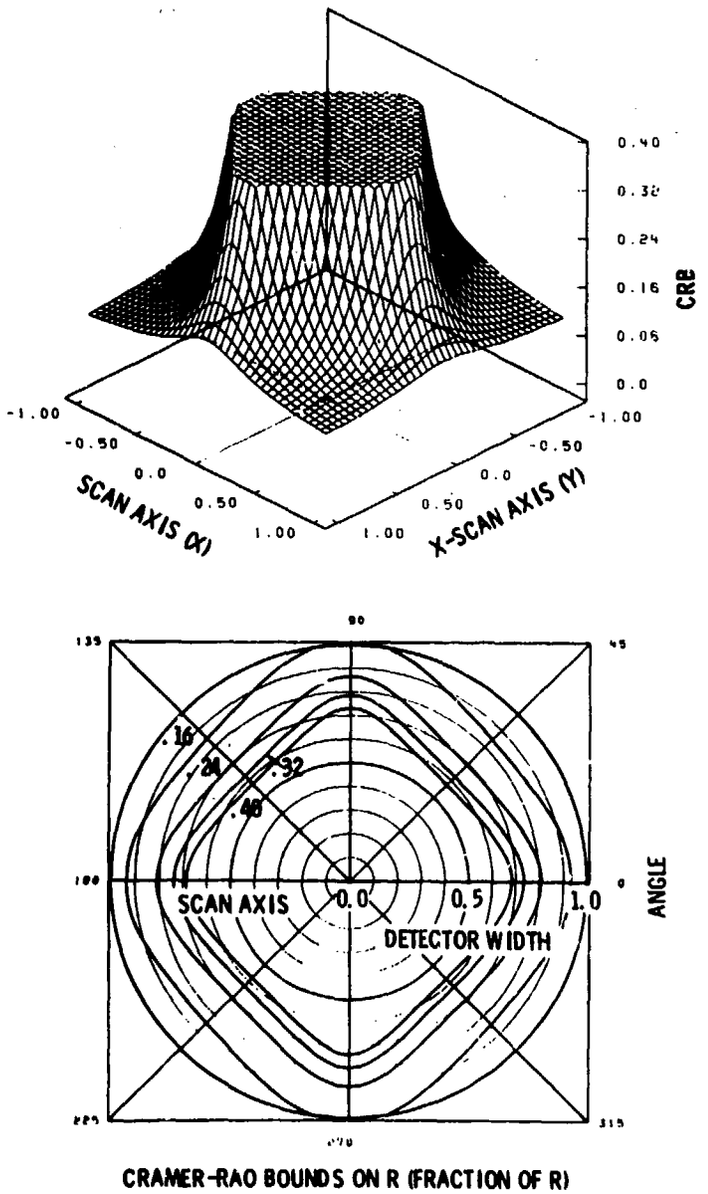

Fig. 8b. The Cramer-Rao bound on the amplitude ratio estimation errors for a crow's foot detector pattern.

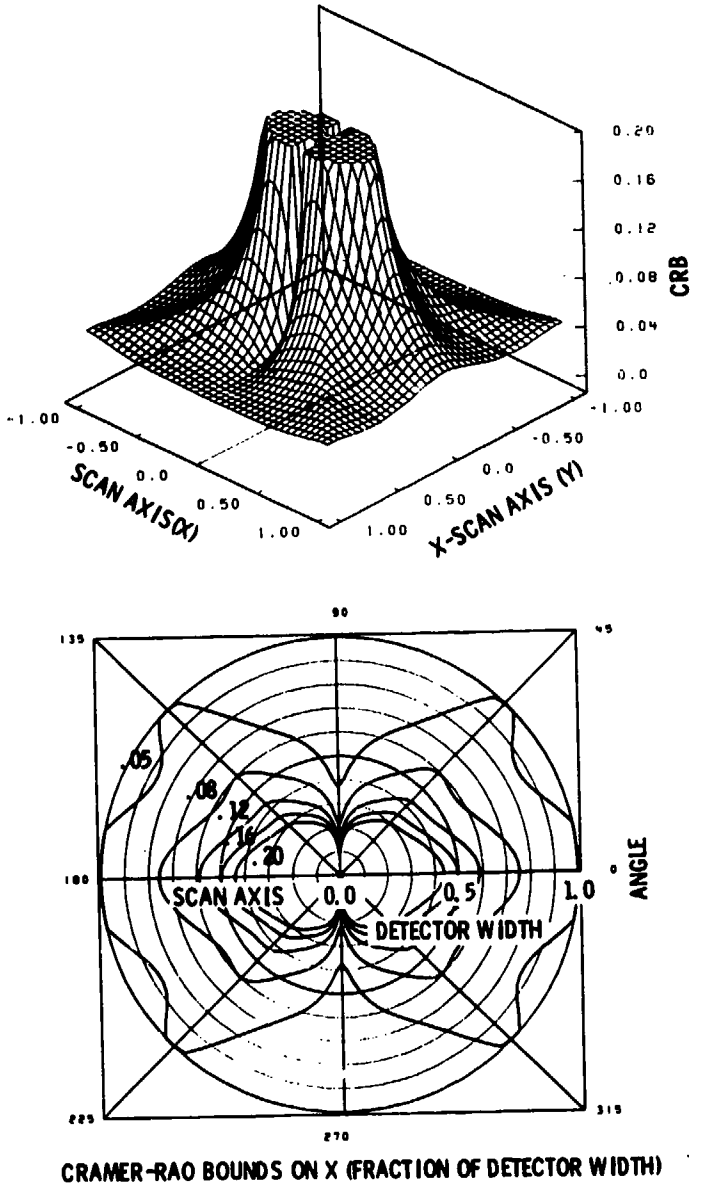

Fig. 8c. The Cramer-Rao bound on the in-scan location estimation errors for a crow's foot detector pattern.

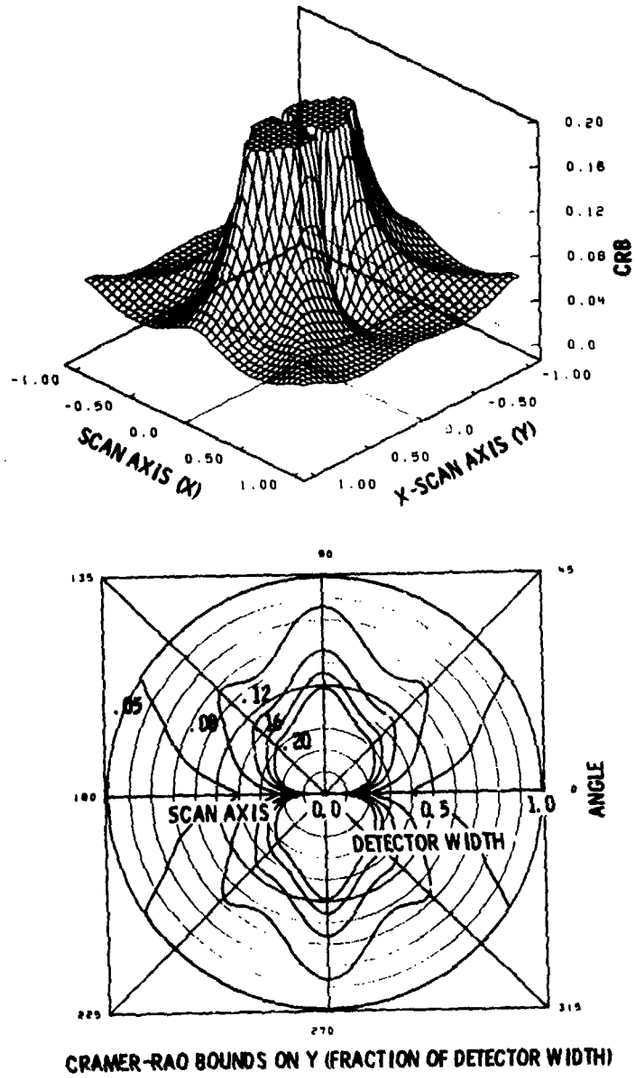

Fig. 8d. The Cramer-Rao bound on the cross-scan location estimation errors for a crow's foot detector pattern.

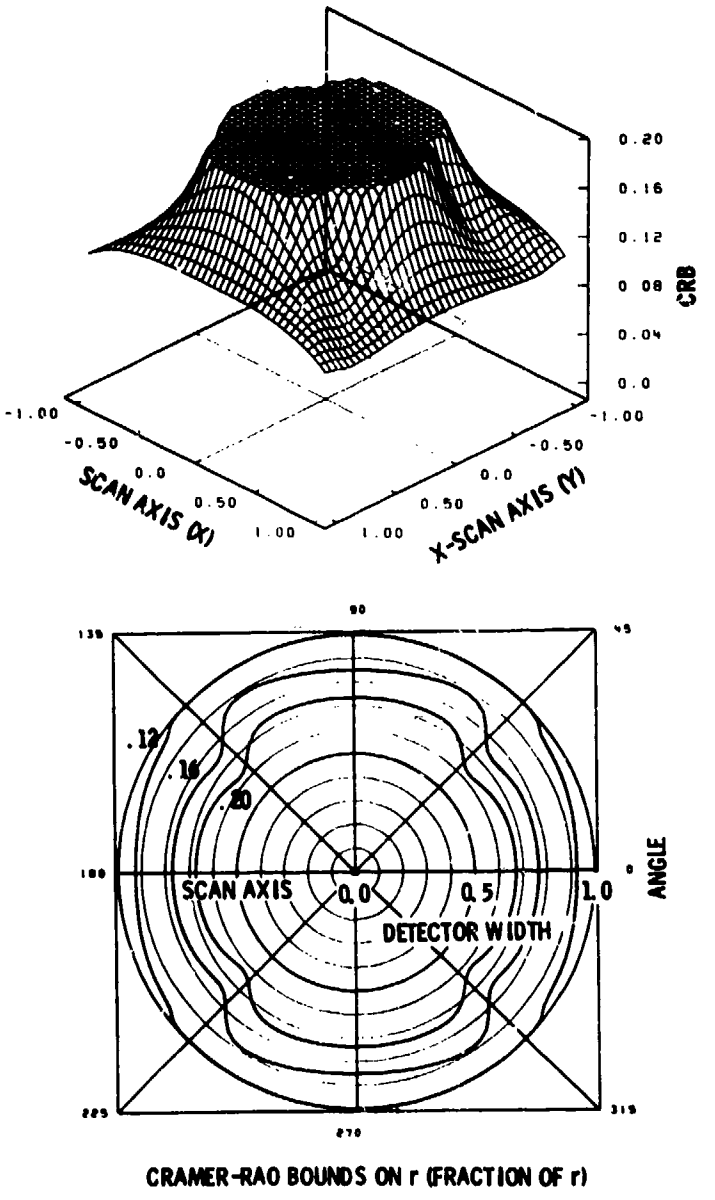

Fig. 8e. The Cramer-Rao bound on the target separation estimation errors for a crow's foot detector pattern.

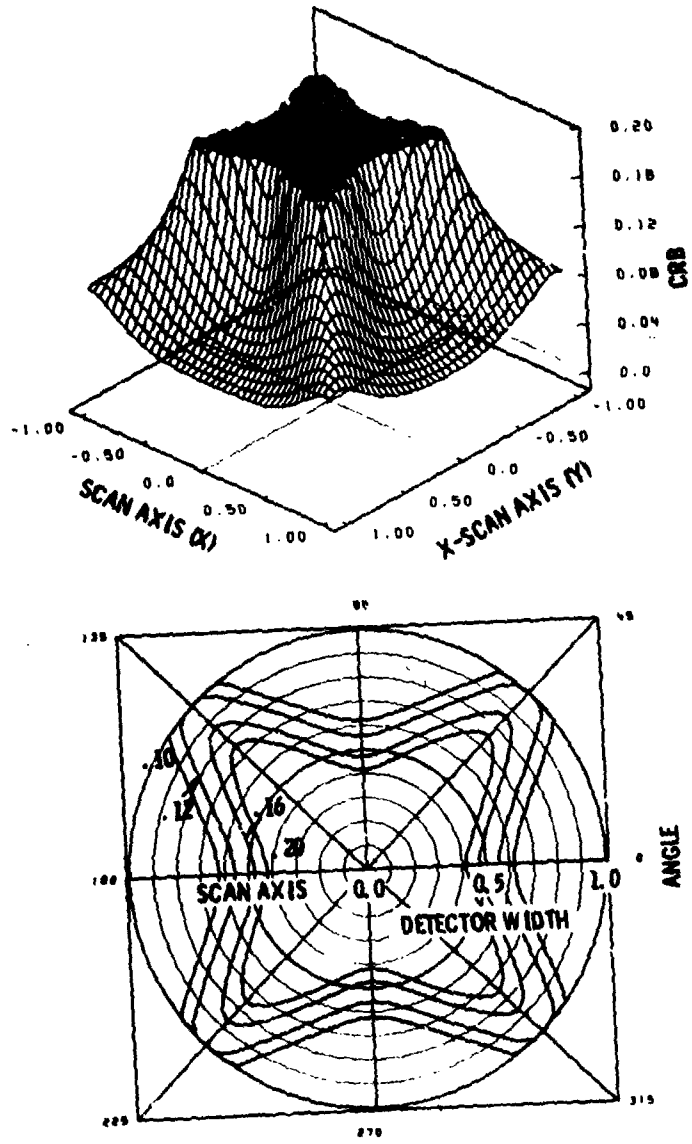

Fig. 8f. The Cramer-Rao bound on the CSO orientation estimation errors for a crow's foot detector pattern.

performance for individual parameters is a function of the information obtained by each detector in the scan direction. For example, the effective target separation measured by the k^{th} detector in the scan direction

$$\Delta x_k = r[\cos\theta - \sin\theta \cot\theta_k] \tag{22}$$

changes as the target pair orientation, θ, changes. Figure 3 shows the detector outputs for three target pair orientations, namely, 0°, 45° and 90°. Table I shows the effective target separation, Δx_k, measured by each detector depicted in Fig. 3 for the three target pairs. From Fig. 6a and 6b we can approximate the estimation errors as a function of Δx_k as follows:

$$\begin{aligned} \sigma^2(a) &= c_1/(\Delta x_k)^2 \\ \sigma^2(\Delta x_k) &= c_2/(\Delta x_k)^2. \end{aligned} \tag{23}$$

The overall estimation performance for a parameter ω, $\sigma(\omega)$, can be approximated as a function of the estimation performance for Δx_k by individual detector outputs, $\sigma_k(\Delta x_k)$. If for simplicity, we ignore the correlation between r and θ, we have

$$\sigma^2(r) \cong \left(\sum_{k=1}^{M} (\cos\theta - \sin\theta \cot\theta_k)^2/\sigma_k^2(\Delta x_k)\right)^{-1} \tag{24}$$

and

$$\sigma^2(\theta) \cong \left(\sum_{k=1}^{M} r^2(\sin\theta + \cos\theta \cot\theta_k)^2/\sigma_k^2(\Delta x_k)\right)^{-1}. \tag{25}$$

Table I also shows the overall estimation performance for a_1, r, and θ using Eqs, (23) - (25).

TABLE I

APPROXIMATE ESTIMATION PERFORMANCE FOR a_1, r, AND θ

Target Pair Orientation	Effective Target Separations			Overall Estimation Performance		
	Δx_1	Δx_2	Δx_3	$\sigma^2(a_1)$	$\sigma^2(r)$	$\sigma^2(\theta)$
0°	r	r	r	$c_1/3r^2$	$c_2/3r^2$	$c_2/2r^4$
45°	0	$r/\sqrt{2}$	$\sqrt{2}r$	$4c_1/17r^2$	$4c_2/17r^2$	$4c_2/r^4$
90°	r	0	r	$c_1/2r^2$	$c_2/2r^2$	$c_2/2r^4$

The approximate estimation performance for a_1, r and θ shown in Table I explains the trend of the equal performance contours presented in Figs. 8a, 8e, and 8f. Thus in Fig. 8a, estimation performance is best at 45° orientation and worst at 90° orientation. It is expected that the estimation performance for R should have a similar pattern to that in Fig. 8a for a_1. Combining the patterns for r and θ observed in Figs. 8e and 8f, one should be able to interpret the patterns shown in Fig. 8c and 8d on x and y, respectively.

This model is oversimplified in that it treats the detectors independently. The analysis used to obtain Figs. 6-8 accounts

for correct combination of individual detectors and thus these results differ from those in Table I.

To summarize the major points for the three classes of detector patterns considered in this section

(1) The linear detector can measure the location of a single target only in the in-scan direction. It can resolve two CSO's only if they are separated in the in-scan direction.

(2) The chevron detector can measure the location of a single target in both the in-scan and cross-scan directions. It can resolve two CSO's if they are separated in either direction but will have degraded performance if their separation direction is aligned with one of the detectors.

(3) The crow's foot detector can measure the location of a single target in both the in-scan and cross-scan directions. It can resolve two CSO's if they are separated in either direction.

(4) For all detector types, the resolution and measurement performance improves with increasing signal-to-noise ratio.

IV. BRICKWALL DETECTOR PATTERNS

In this section, the detector array consists of M rectangular detectors with $\theta_k = 90°$. The center of each detector is not necessary located along the scan axis as shown in Fig. 2. For simplicity, let us assume that the output of each detector to a unit strength point source located at (x,y) has the same functional form:

$$p_k(t, x, y) = p_x(t-x+x_k)p_y(y_k-y) \tag{26}$$

where $p_x(\cdot)$, $p_y(\cdot)$ are symmetric, nonnegative-valued functions and (x_k, y_k) is the center of the kth detector. Let $\rho(t)$ be the autocorrelation function of $p_x(t)$, i.e.,

$$\rho(t) = \int_{-\infty}^{\infty} p_x(\tau)p_x(\tau-t)d\tau. \tag{27}$$

Rewriting (3) in terms of the parameters considered in Section II with the above assumptions, we have

$$s_k(t) = a_1 p_x(t-\bar{x}_1+x_k)p_y(y_k-\bar{y}_1) + a_2 p_x(t-\bar{x}_1-r\cos\theta+x_k)p_y(y_k-\bar{y}_1-r\sin\theta). \tag{28}$$

Substituting (28) into (9), we have F_{ij} in terms of ρ, $\dot{\rho}$, $\ddot{\rho}$, p_y, and $\dot{p}_y$. The expression for each element of F is given in Appendix B. The lower bounds on the variances of the estimates for a_1, R, $\bar{x}_1$, $\bar{y}_1$, r, and θ are the diagonal elements of the inverse of the Fisher information matrix, F, as in Eqs. (16a) - (16f) of Section III.

The results presented in this section are values of the normalized errors defined in Eqs. (17a) - (17f) in the last section. All results are presented at SNR_1=10 of target No. 1. SNR_1 is defined in (18a) with

$$\sigma_a \triangleq p_y(0)\left[\int_{-\infty}^{\infty} p_x^2(t)dt\right]^{1/2} = 1. \qquad (29)$$

For a different signal-to-noise ratio, the same formula given in (19) applies. The same point spread function (Eqs. (20)-(21)) is used in the numerical examples presented here.

Figures 9a - 9f present the Cramer-Rao bounds on the estimation errors defined in Eqs. (17a) - (17f) for a brickwall detector pattern shown in Fig. 10. The results presented here are very similar to those shown in Figs. 8a - 8f for the crow's foot pattern in terms of the shape of the equal performance contours. Notice that for the same signal-to-noise ratio for each detector in both patterns* the overall signal-to-noise ratio of the brickwall pattern is lower than that of the crow's foot pattern. For example, for a target located along the scan axis (x-axis), the ratio is about 1.5 to 1. This difference should be taken into account when a comparison of parameter estimation performance between these two patterns is made. The amplitude of each detector output to a unit strength point source is a function of the cross-scan separation between the point source and the

*To achieve the same SNR per detector requires matching the blur circle to the smaller detector size in the brickwall pattern.

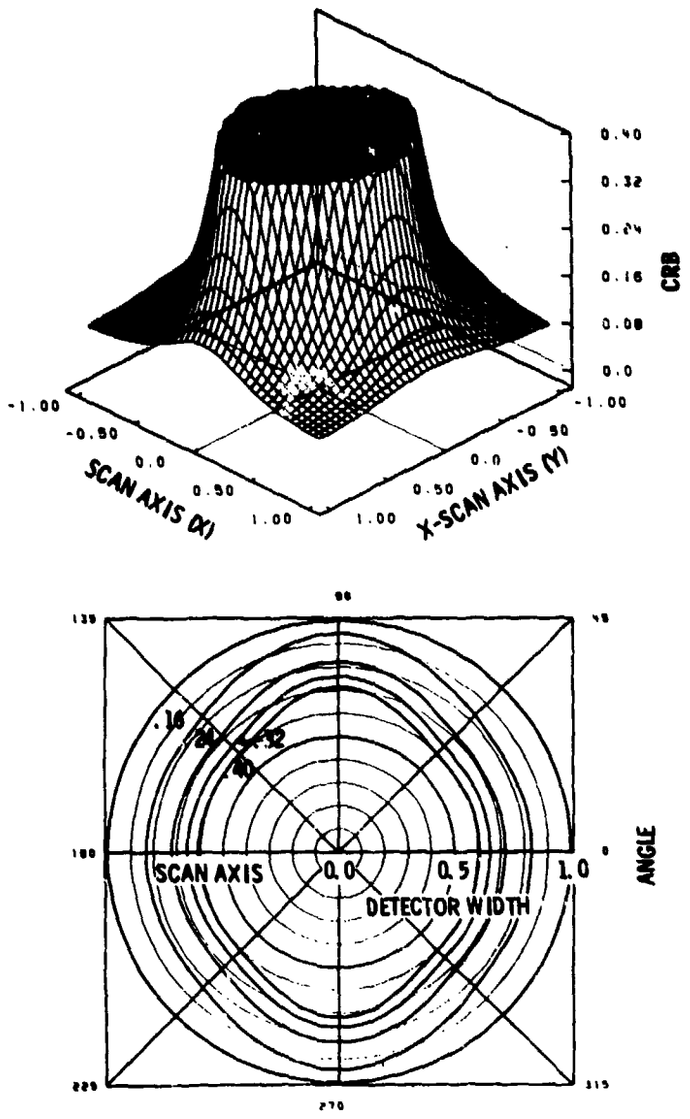

Fig. 9a. The Cramer-Rao bound on the amplitude estimation errors for a 5-detector brickwall pattern.

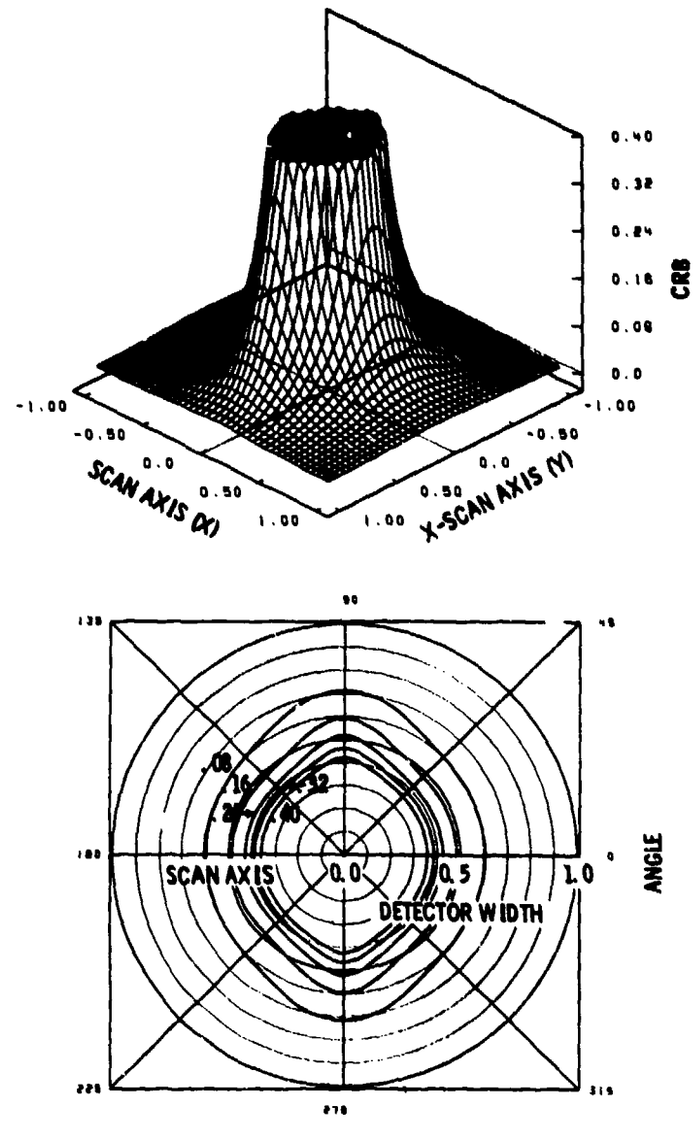

Fig. 9b. The Cramer-Rao bound on the amplitude ratio estimation errors for a 5-detector brickwall pattern.

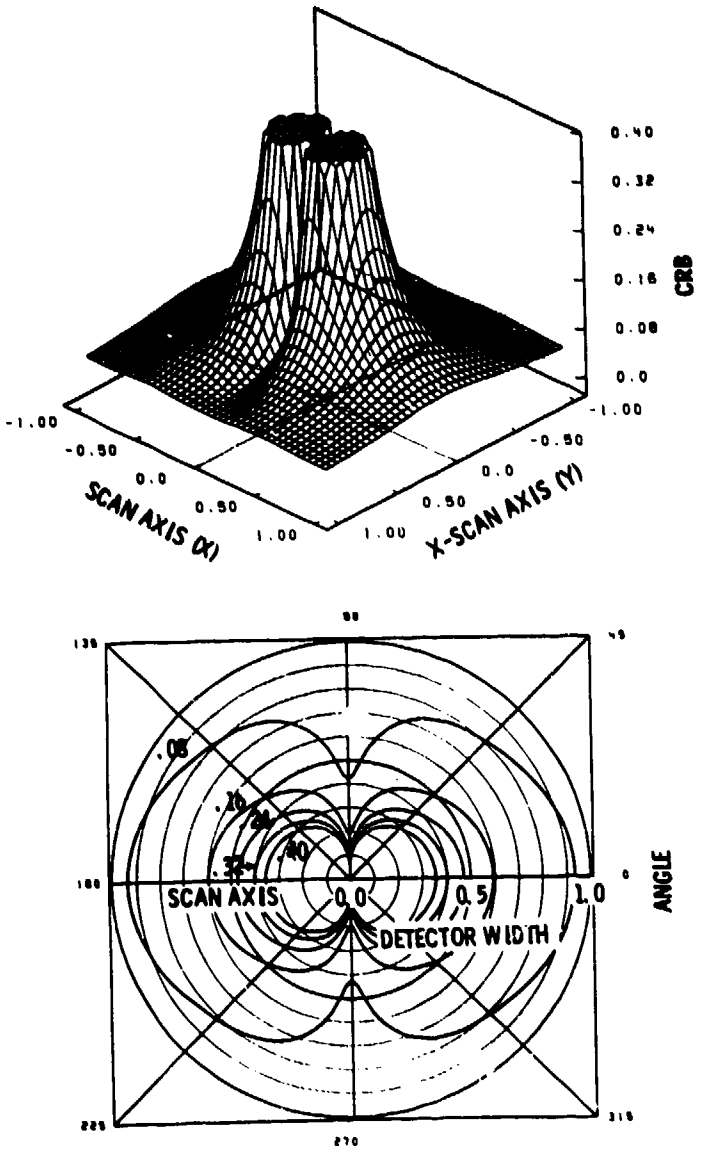

Fig. 9c. The Cramer-Rao bound on the in-scan location estimation errors for a 5-detector brickwall pattern.

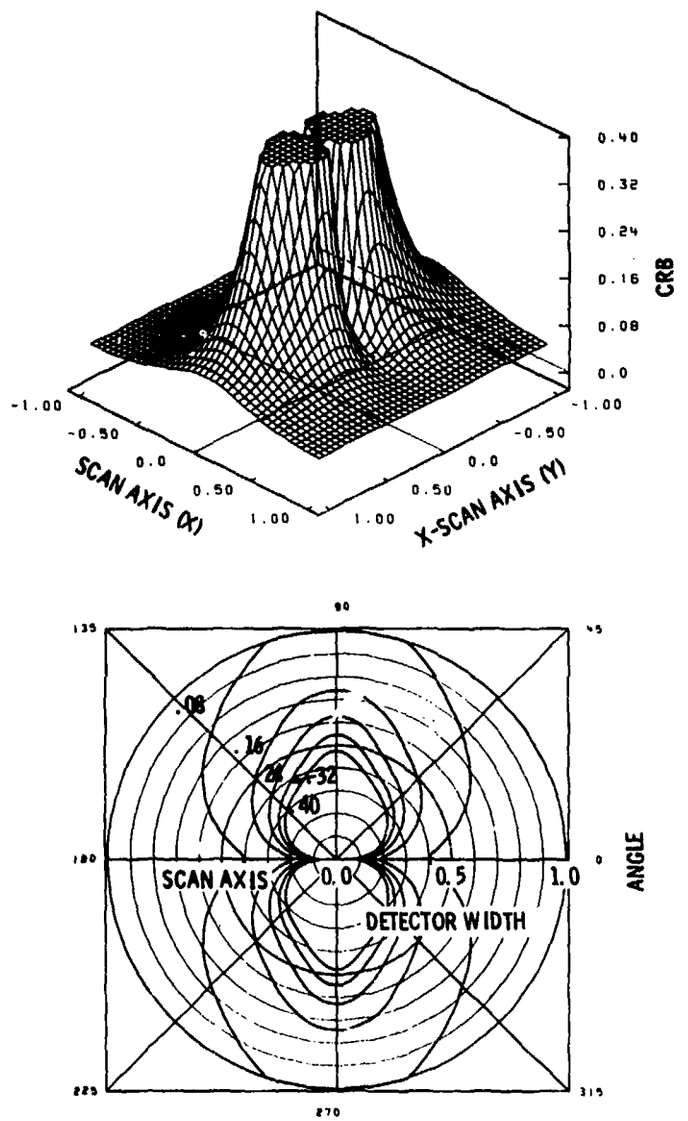

Fig. 9d. The Cramer-Rao bound on the cross-scan location estimation errors for a 5-detector brickwall pattern.

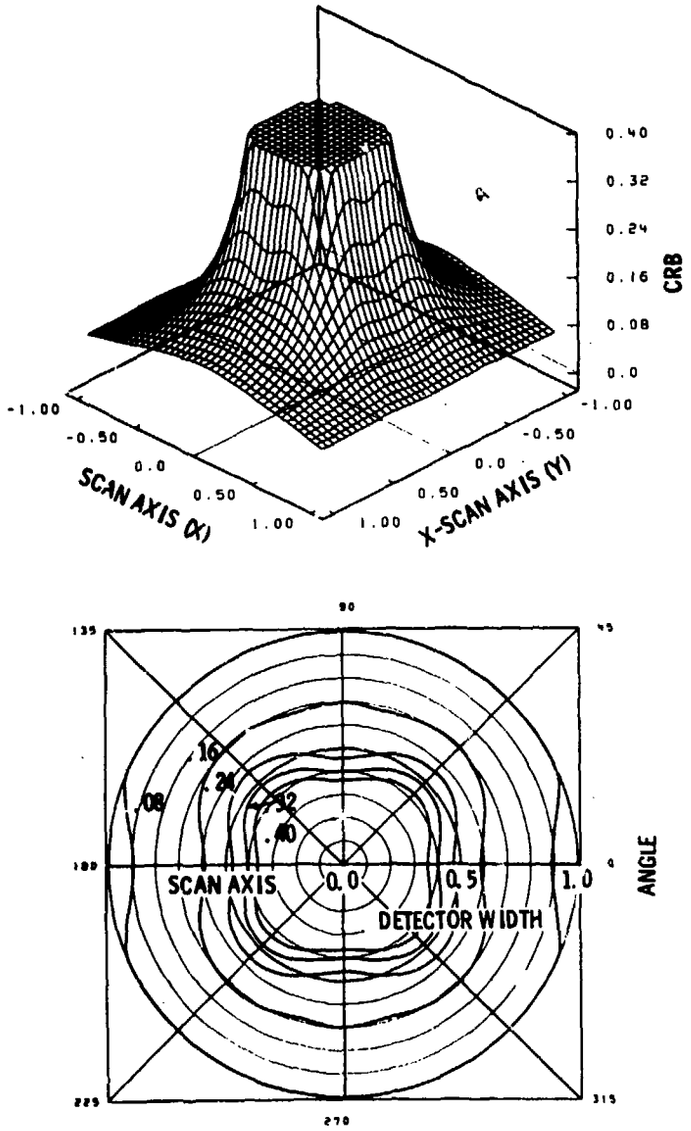

Fig. 9e. The Cramer-Rao bound on the target separation estimation errors for a 5-detector brickwall pattern.

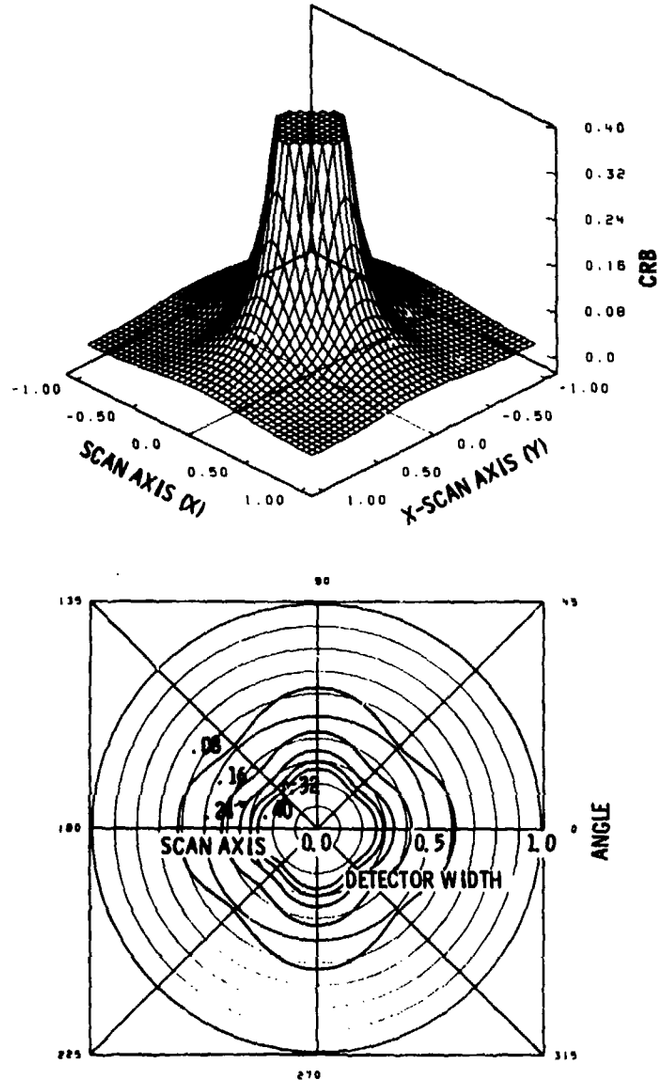

Fig. 9f. The Cramer-Rao bound on the CSO orientation estimation errors for a 5-detector brickwall pattern.

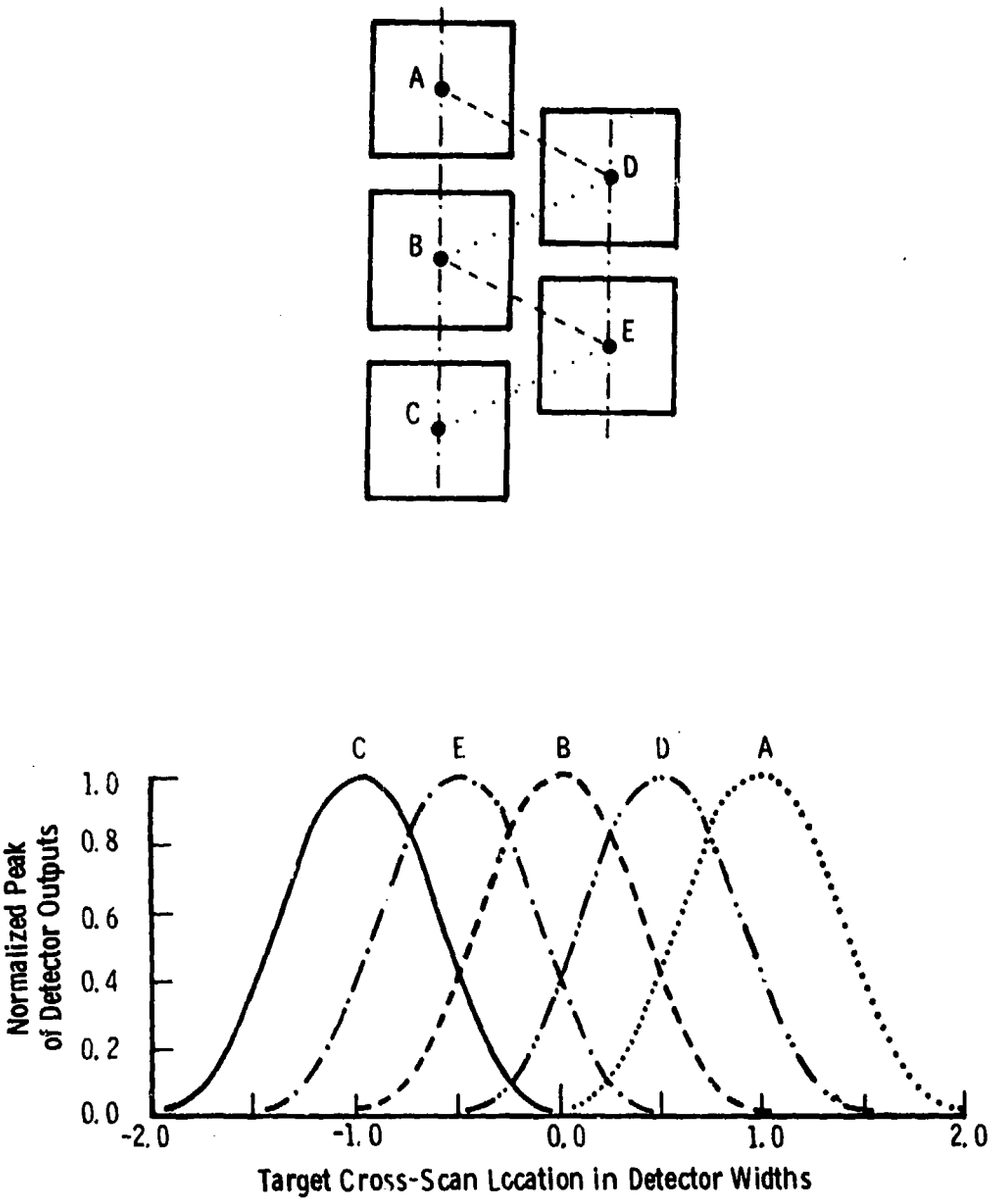

Fig. 10. The 5-detector brickwall pattern and the normalized peak of each individual detector as a function of target cross-scan location.

center of the detector as indicated in Eq. (26). The normalized peak amplitdue of each detector output is plotted as a function of the cross-scan target location in Fig. 10 for the detector pattern shown in the figure. The brickwall pattern differs from the previous chevron and crow's foot patterns in using amplitude rather than separation estimates from individual detectors to obtain information on target separation in the cross-scan direction. In spite of this difference, the resulting performance is quite similar to that achieved by the crow's foot.

The brickwall pattern occupies much less area on the focal plane than does the crow's foot pattern. However to achieve the performance presented in Fig. 9, optimal signal processing of the outputs of at least 5 detectors was assumed. Simpler suboptimal processing may be carried out by combining adjacent detectors as shown by the dotted lines in Fig. 10. In this way, a crow's foot pattern may be synthesized from the mosaic pattern.

V. DISCUSSION AND SUMMARY

In this report, we have derived the Cramer-Rao lower bounds on the variances of parameter estimates for two CSOs separated in both the in-scan and the cross-scan direction as measured by two classes of detector patterns. Numerical results are presented for a particular point spread function and a fixed detector width in the scan direction for both detector patterns. The trends of the equi-performance contours of each parameter of interest for both patterns are quite similar. For the cases considered in this report, the achievable parameter estimation performance of the 5-detector brickwall (mosaic) pattern is, in general, poorer than the 3-detector crow's foot patterns for targets with SNR of 10 per detector. This is because the overall received SNR of the particular brickwall (mosaic) pattern considered is lower than that of the crow's foot pattern. To achieve the same performance using the mosaic pattern would require more detector columns (>2) as well as a greater signal processing load. However, the brickwall (mosaic) pattern may still require a smaller focal plane area to achieve the same performance as the simple crow's foot pattern.

We have not implemented an algorithm to do 2-dimensional CSO detection and parameter estimation. No simulation performance results have been obtained to compare with the theoretical bounds presented here. The signal processing load for the 2-D problem increases as a power of the number of detectors in the pattern, if

an optimal performance algorithm is implemented. For a sub-optimal algorithm, the predicted performance presented here may not be easy to achieve. This is an area which requires further investigation.

General trends in estimation performance were summarized at the ends of Section III and IV.

APPENDIX A. THE FISHER INFORMATION MATRIX FOR LINEAR, CHEVRON, AND CROW'S FOOT DETECTOR ARRAYS

Let

$$s_k(t) = a_1 p(t-\tau_k) + a_1 R p(t-\tau_k-\Delta_k), \tag{A.1}$$

where

$$\tau_k = \bar{x}_1 - x_k - \bar{y}_1 \cot\theta_k \tag{A.2}$$

and

$$\Delta_k = r\cos\theta - r\sin\theta\cot\theta_k. \tag{A.3}$$

Then, the derivatives of s_k are:

$$\frac{\partial s_k(t)}{\partial a_1} = p(t-\tau_k) + Rp(t-\tau_k-\Delta_k), \tag{A.4a}$$

$$\frac{\partial s_k(t)}{\partial R} = a_1 p(t-\tau_k-\Delta_k), \tag{A.4b}$$

$$\frac{\partial s_k(t)}{\partial \bar{x}_1} = -a_1[\dot{p}(t-\tau_k) + R\dot{p}(t-\tau_k-\Delta_k)], \tag{A.4c}$$

$$\frac{\partial s_k(t)}{\partial \bar{y}_1} = a_1\cot\theta_k[\dot{p}(t-\tau_k) + R\dot{p}(t-\tau_k-\Delta_k)], \tag{A.4d}$$

$$\frac{\partial s_k(t)}{\partial r} = -a_1 R(\cos\theta - \sin\theta\cot\theta_k)\dot{p}(t-\tau_k-\Delta_k), \tag{A.4e}$$

$$\frac{\partial\, s_k(t)}{\partial\, \theta} = a_1 R\, r(\sin\theta + \cos\theta\, \cot\theta_k)\dot{p}(t-\tau_k-\Delta_k), \qquad \text{(A.4f)}$$

where $\dot{p}(t)$ is the 1st order derivative of p(t) with respect to t. Substituting (A.4a) - (A.4f) into (9) and rewriting it in terms of the following functions:

$$\rho(\tau) = \int_{-\infty}^{\infty} p(t)p(t-\tau)dt, \qquad \text{(A.5a)}$$

$$\dot{\rho}(\tau) = -\int_{-\infty}^{\infty} \dot{p}(t)p(t-\tau)dt, \qquad \text{(A.5b)}$$

and

$$\ddot{\rho}(\tau) = -\int_{-\infty}^{\infty} \dot{p}(t)\dot{p}(t-\tau)dt, \qquad \text{(A.5c)}$$

we have

$$F_{ij} = \frac{2}{N_o} \sum_{k=1}^{M} (f_{ij})k \qquad \text{for } i,j=1,2,..,6 \qquad \text{(A.6)}$$

where

$$(f_{11})_k = (1+R^2)\rho(0) + 2R\rho(\Delta_k) \qquad \text{(A.7a)}$$

$$(f_{12})_k = a_1\rho(\Delta_k) + a_1 R\, \rho(0) \qquad \text{(A.7b)}$$

$$(f_{15})_k = a_1 R(\cos\theta - \sin\theta\cot\theta_k)\dot{\rho}(\Delta_k) \qquad \text{(A.7c)}$$

$$(f_{16})_k = -a_1 R\, r(\sin\theta + \cos\theta\cot\theta_k)\dot{\rho}(\Delta_k) \qquad \text{(A.7d)}$$

$$(f_{22})_k = a_1^2\rho(0) \qquad \text{(A.7e)}$$

$$(f_{23})_k = -a_1^2\, \dot{\rho}(\Delta_k) \qquad \text{(A.7f)}$$

$$(f_{24})_k = a_1^2 \cot\theta_k \, \dot{\rho}(\Delta_k) \tag{A.7g}$$

$$(f_{33})_k = -a_1^2(1+R^2)\ddot{\rho}(0) - 2a_1^2 R\ddot{\rho}(\Delta_k) \tag{A.7h}$$

$$(f_{34})_k = -\cot\theta_k (f_{33})_k \tag{A.7i}$$

$$(f_{35})_k = -a_1^2 R(\cos\theta - \sin\theta\cot\theta_k)[\dot{\rho}(\Delta_k) + R\dot{\rho}(0)] \tag{A.7j}$$

$$(f_{36})_k = a_1^2 Rr(\sin\theta + \cos\theta\cot\theta_k)[\dot{\rho}(\Delta_k) + R\dot{\rho}(0)] \tag{A.7k}$$

$$(f_{44})_k = -\cot\theta_k (f_{34})_k \tag{A.7l}$$

$$(f_{45})_k = -\cot\theta_k (f_{35})_k \tag{A.7m}$$

$$(f_{46})_k = -\cot\theta_k (f_{36})_k \tag{A.7n}$$

$$(f_{55})_k = -a_1^2 R^2(\cos\theta - \sin\theta\cot\theta_k)^2 \ddot{\rho}(0) \tag{A.7o}$$

$$(f_{56})_k = a_1^2 R^2 r(\cos\theta - \sin\theta\cot\theta_k)(\sin\theta + \cos\theta\cot\theta_k)\ddot{\rho}(0) \tag{A.7p}$$

$$(f_{66})_k = -a_1^2 R^2 r^2(\sin\theta + \cos\theta\cot\theta_k)^2 \ddot{\rho}(0) \tag{A.7q}$$

and

$$(f_{13})_k = (f_{14})_k = (f_{25})_k = (f_{26})_k = 0$$

where $\dot{\rho}$ and $\ddot{\rho}$ are the 1st and 2nd order derivatives of ρ, respectively. Inverting this 6 x 6 symmetric matrix, F, one should be able to obtain the Cramer-Rao lower bound on the estimates as shown in (16a) - (16f) of Section III.

APPENDIX B. THE FISHER INFORMATION MATRIX FOR BRICKWALL DETECTOR PATTERNS

Let

$$s_k(t) = a_1 p_x(t-\tau_k)p_y(y_k-\bar{y}_1) + a_1 R p_x(t-\tau_k-r\cos\phi)p_y(y_k-\bar{y}_1-r\sin\phi) \tag{B.1}$$

where

$$\tau_k = \bar{x}_1 - x_k. \tag{B.2}$$

Then, the derivatives of s_k are:

$$\frac{\partial s_k(t)}{\partial a_1} = p_x(t-\tau_k)p_y(y_k-\bar{y}_1) + R p_x(t-\tau_k-r\cos\theta)p_y(y_k-\bar{y}_1-r\sin\theta), \tag{B.3a}$$

$$\frac{\partial s_k(t)}{\partial R} = a_1 p_x(t-\tau_k-r\cos\theta)\ p_y(y_k-\bar{y}_1-\sin\theta), \tag{B.3b}$$

$$\frac{\partial s_k(t)}{\partial \bar{x}_1} = -a_1\dot{p}_x(t-\tau_k)p_y(y_k-\bar{y}_1) - a_1 R\dot{p}_x(t-\tau_k-r\cos\theta)p_y(y_k-\bar{y}_1-r\sin\theta), \tag{B.3c}$$

$$\frac{\partial s_k(t)}{\partial \bar{y}_1} = -a_1 p_x(t-\tau_k)\dot{p}_y(y_k-\bar{y}_1) - a_1 R p_x(t-\tau_k-r\cos\theta)\dot{p}_y(y_k-\bar{y}_1-r\sin\theta), \tag{B.3d}$$

$$\frac{\partial s_k(t)}{\partial r} = -a_1 R\cos\theta\dot{p}_x(t-\tau_k-r\cos\theta)p_y(y_k-\bar{y}_1-r\sin\theta) - a_1 R r\sin\theta p_x(t-\tau_k-r\cos\theta)\dot{p}_y(y_k-\bar{y}_1-r\sin\theta), \tag{B.3e}$$

$$\frac{\partial s_k(t)}{\partial \theta} = a_1 R r \sin\theta \dot{p}_x(t-\tau_k-r\cos\theta) p_y(y_k-\bar{y}_1-r\sin\theta)$$
$$-a_1 R r\cos\theta p_x(t-\tau_k-r\cos\theta)\dot{p}_y(y_k-y_1-r\sin\theta), \qquad \text{(B.3f)}$$

where $\dot{p}_x(\cdot)$ and $\dot{p}_y(\cdot)$ are the 1st order derivatives of p_x and p_y, respectively. For notational simplicity, we will use p_1 and p_2 in the rest of this Appendix to denote $p_y(y_k-\bar{y}_1)$ and $p_y(y_k-\bar{y}_1-r\sin\theta)$, respectively.

Substituting (B.3a) - (B.3f) into (9) and rewriting it in terms of ρ, the autocorrelation function of p_x defined by (11), and its derivatives $\dot{\rho}$, and $\ddot{\rho}$, we have

$$F_{ij} = \frac{2}{N_o}\sum_{k=1}^{M}(f_{ij})_k, \qquad \text{for } i,j = 1,2,\ldots,6 \qquad \text{(B.4)}$$

where

$$(f_{11})_k = (p_1^2+p_2^2R^2)\rho(0) + 2p_1p_2R\rho(r\cos\theta) \qquad \text{(B.5a)}$$

$$(f_{12})_k = a_1p_1p_2\rho(r\cos\theta) + a_1Rp_2^2\rho(0) \qquad \text{(B.5b)}$$

$$(f_{14})_k = -a_1(\rho_1\dot{p}_1+R^2p_2\dot{p}_2)\rho(0) - a_1R(\dot{p}_1p_2+p_1\dot{p}_2)\rho(r\cos\theta) \qquad \text{(B.5c)}$$

$$(f_{15})_k = a_1Rp_1p_2\cos\theta\dot{\rho}(r\cos\theta) - a_1Rp_1\dot{p}_2\sin\theta\rho(r\cos\theta)$$
$$-a_1R^2p_2\dot{p}_2\sin\theta\rho(0) \qquad \text{(B.5d)}$$

$$(f_{16})_k = -a_1Rrp_1p_2\sin\theta\dot{\rho}(r\cos\theta) - a_1Rrp_1\dot{p}_2\cos\theta\rho(r\cos\theta)$$
$$-a_1R^2rp_2\dot{p}_2\cos\theta\rho(0) \qquad \text{(B.5e)}$$

$$(f_{22})_k = a_1^2 p_2^2 \rho(0) \tag{B.5f}$$

$$(f_{23})_k = -a_1^2 p_1 p_2 \dot{\rho}(r\cos\theta) \tag{B.5g}$$

$$(f_{24})_k = -a_1^2 \dot{p}_1 p_2 \rho(r\cos\theta) - a_1^2 R p_2 \dot{p}_2 \rho(0) \tag{B.5h}$$

$$(f_{25})_k = -a_1^2 R p_2 \dot{p}_2 \sin\theta \rho(0) \tag{B.5i}$$

$$(f_{26})_k = -a_1^2 R r p_2 \dot{p}_2 \cos\theta \rho(0) \tag{B.5j}$$

$$(f_{33})_k = -a_1^2 (p_1^2 + p_2^2 R^2) \ddot{\rho}(0) - 2a_1^2 R p_1 p_2 \ddot{\rho}(r\cos\theta) \tag{B.5k}$$

$$(f_{34})_k = a_1^2 R (p_1 \dot{p}_2 - \dot{p}_1 p_2) \dot{\rho}(r\cos\theta) \tag{B.5l}$$

$$(f_{35})_k = -a_1^2 R p_1 p_2 \cos\theta \ddot{\rho}(r\cos\theta) - a_1^2 R^2 p_2^2 \cos\theta \ddot{\rho}(0) + a_1^2 R p_1 \dot{p}_2 \sin\theta \dot{\rho}(r\cos\theta) \tag{B.5m}$$

$$(f_{36})_k = a_1^2 R r p_1 p_2 \sin\theta \ddot{\rho}(r\cos\theta) + a_1^2 R r p_1 \dot{p}_2 \cos\theta \dot{\rho}(r\cos\theta) + a_1^2 R^2 r p_2^2 \sin\theta \ddot{\rho}(0) \tag{B.5n}$$

$$(f_{44})_k = (a_1^2 \dot{p}_1^2 + a_1^2 R^2 \dot{p}_2^2) \rho(0) + 2a_1^2 R \dot{p}_1 \dot{p}_2 \rho(r\cos\theta) \tag{B.5o}$$

$$(f_{45})_k = -a_1^2 R \dot{p}_1 p_2 \cos\theta \dot{\rho}(r\cos\theta) + a_1^2 R \dot{p}_1 \dot{p}_2 \sin\theta \rho(r\cos\theta) + a_1^2 R^2 \dot{p}_2^2 \sin\theta \rho(0) \tag{B.5p}$$

$$(f_{46})_k = a_1^2 R r \dot{p}_1 p_2 \sin\theta \dot{\rho}(r\cos\theta) + a_1^2 R r \dot{p}_1 \dot{p}_2 \cos\theta \rho(r\cos\theta) + a_1^2 R^2 r \dot{p}_2^2 \cos\theta \rho(0) \tag{B.5q}$$

$$(f_{55})_k = -a_1^2 R^2 \left[\cos^2\theta p_2^2 \ddot{\rho}(0) - \sin^2\theta \dot{p}_2^2 \rho(0)\right] \tag{B.5r}$$

$$(f_{56})_k = a_1^2 R^2 r \sin\theta\cos\theta\left[p_2^2\ddot{\rho}(0) + \dot{p}_2^2\rho(0)\right] \tag{B.5s}$$

$$(f_{66})_k = -a_1^2 R^2 r^2\left[p_2^2\sin^2\theta\ddot{\rho}(0) - \dot{p}_2^2\cos^2\theta\rho(0)\right] \tag{B.5t}$$

ACKNOWLEDGMENTS

The author would like to thank Dr. S. D. Weiner for his critical comments and careful reviews. The author also wishes to thank Frances Chen for her programming assistance, and personally acknowledge C. A. Tisdale for patiently typing this report and all its revisions.

REFERENCES

1. D. L. Fried, "Resolution, Signal-to-Noise Ratio and Measurement Precision," Optical Science Consultants, Report No. TR-034, (October 1971), also published in J. Opt. Soc. Am., 69, 399 (1979).

2. R. W. Miller, "Accuracy of Parameter Estimates for Unresolved Objects," Technical Note 1978-20, Lincoln Laboratory M.I.T. (8 June 1978), DDC AD-B028168.

3. M. J. Tsai and K. P. Dunn, "Performance Limitation on Parameter Estimation of Closely Spaced Optical Targets Using Shot-Noise Detector Model," Technical Note 1979-35, Lincoln Laboratory, M.I.T. (13 June 1979), DDC AD-A073462.

4. K. P. Dunn, "Accuracy of Parameter Estimates for Closely Spaced Optical Targets," Technical Note 1979-43, Lincoln Laboratory, M.I.T. (13 June 1979), DDC AD-A073093.

5. M. J. Tsai, "Simulation Study on Detection and Estimation of Closely Spaced Optical Targets," Technical Note 1980-19, Lincoln Laboratory, M.I.T. (18 March 1980), DTIC-AD-A088098/9.

6. D. L. Fried, "Distinguishing Between a Single Object and Closely Spaced Objects: Signal Processing Analysis," the Optical Science Company, Report No. TR-299, (February 1978).

7. Y. Kimashi, "Dual Pulse Matcher Performance Analysis," Passive Optical Algorithm Development for Layered Defense Program, Nichols Research Corporation, Report No. NRC-LDST-017A (1 October 1978).

8. H. Akaike, "A New Look at the Statistical Model Identification," IEEE. Trans. Automat. Contr. AC-19, 716 (1974).

9. H. L. Van Trees, Detection, Estimation and Modulation Theory, Part I, (Wiley, New York 1968).

10. K. Seyrafi, Electro-Optical Systems Analysis, (Electro-Optical Research Compnay, Los Angeles, 1973).

UNCLASSIFIED

SECURITY CLASSIFICATION OF THIS PAGE *(When Data Entered)*

REPORT DOCUMENTATION PAGE		READ INSTRUCTIONS BEFORE COMPLETING FORM
1. REPORT NUMBER (11) ESD-TR-81-292	2. GOVT ACCESSION NO. AD-A109 285	3. RECIPIENT'S CATALOG NUMBER
4. TITLE *(and Subtitle)* Accuracy of Parameter Estimates for Closely Spaced Optical Targets Using Multiple Detectors		5. TYPE OF REPORT & PERIOD COVERED Technical Report
		6. PERFORMING ORG. REPORT NUMBER Technical Report 589
7. AUTHOR(s) Keh-Ping Dunn (11) TR-589		8. CONTRACT OR GRANT NUMBER(s) F19628-80-C-0002
9. PERFORMING ORGANIZATION NAME AND ADDRESS Lincoln Laboratory, M.I.T. P.O. Box 73 Lexington, MA 02173		10. PROGRAM ELEMENT, PROJECT, TASK AREA & WORK UNIT NUMBERS Program Element No. 63308A
11. CONTROLLING OFFICE NAME AND ADDRESS Air Force Systems Command, USAF Andrews AFB Washington, DC 20331		12. REPORT DATE 23 October 1981
		13. NUMBER OF PAGES 58
14. MONITORING AGENCY NAME & ADDRESS *(if different from Controlling Office)* Electronic Systems Division Hanscom AFB Bedford, MA 01731		15. SECURITY CLASS. *(of this report)* Unclassified
		15a. DECLASSIFICATION DOWNGRADING SCHEDULE

16. DISTRIBUTION STATEMENT *(of this Report)*

Approved for public release; distribution unlimited.

17. DISTRIBUTION STATEMENT *(of the abstract entered in Block 20, if different from Report)*

18. SUPPLEMENTARY NOTES

None

19. KEY WORDS *(Continue on reverse side if necessary and identify by block number)*

Cramer-Rao bound
closely spaced objects
parameter estimation
passive optical sensors
degradation
multiple detectors

20. ABSTRACT *(Continue on reverse side if necessary and identify by block number)*

In order to obtain the cross-scan position of an optical target, more than one scanning detectors are used. As expected, the cross-scan position estimation performance degrades when two nearby optical targets interfere with each other. Theoretical bounds on the two-dimensional parameter estimation performance for two closely spaced optical targets are found. Two particular classes of scanning detector arrays, namely, the crow's foot and the brickwall (or mosaic) patterns, are considered.

DD FORM 1 JAN 73 1473 EDITION OF 1 NOV 65 IS OBSOLETE

UNCLASSIFIED

SECURITY CLASSIFICATION OF THIS PAGE *(When Data Entered)*